JET-P(96)16

Thermal Transport from a Phenomenological Description of Ion-Temperature-Gradient-Driven Turbulence

M Ottaviani, W Horton[1], M Erba.

JET Joint Undertaking, Abingdon, Oxfordshire, OX14 3EA, UK.
[1] IFS, University of Texas at Austin, Austin, TX 78712-1060, USA.

Preprint of a paper to be submitted for application in
Plasma Physics and Controlled Fusion

May 1996

ABSTRACT

In this work a phenomenological model of the thermal transport caused by ion-temperature-gradient-driven turbulence is introduced. A relevant property of the model is that the thermal conductivities grow with minor radius, due to the positive dependence of the correlation length and of the inverse timescale on the ion temperature gradient. A comparison of the predicted profiles with the experimental ones of several machines is presented.

1. INTRODUCTION

A substantial amount of theoretical effort has been oriented towards understanding anomalous transport in tokamaks. *Ab initio* calculations of transport caused by various forms of plasma turbulence has been the prevailing attempted route in a couple of decades of anomalous transport research. Unfortunately, insufficient understanding of the basic mechanisms of plasma turbulence coupled with the complexity of the problem at hand has frustrated all the attempts at producing a convincing model of thermal transport that agrees satisfactorily with the experiments. In this respect, a well-known difficulty has been the radial dependence of the conductivity, which is found to increase towards the plasma edge, but which available models usually predict to be a decreasing function.

It is therefore understandable that the attention of researchers in recent years has turned to phenomenological models, helped in this quest by increasingly detailed and more carefully designed experiments.

In this work, we combine the semi-quantitative knowledge of microturbulence so far accumulated with information drawn from the experiments to propose formulas for the ion and electron heat conductivities. We then carry out a comparison of the prediction of our model as obtained by simulating transport with the JETTO code [1] with the experimental profiles of a number of machines (JET, TFTR, JT-60, D-III-D, ASDEX-U and START).

The plan of this work is as follows. In Section 2 the transport model is introduced and justified. Some general properties of the model are discussed in Section 3 where it is also shown how the model is consistent with dimensional analysis of a simple ITG model. Comparison with the experiments is presented in Section 4 and conclusions in Section 5.

2. DERIVATION OF THE TRANSPORT MODEL

The relatively good thermal confinement properties of tokamaks among various toroidal devices can be attributed to the axisymmetric design combined with good stability properties to magnetic perturbations. In this way, losses along stray field lines associated with the breaking of axisymmetry are kept to a minimum and are generally radially localised around the region where

low-m macroscopic magnetic islands occasionally appear. Thus the incremental transport caused by such a structure is small and cannot account for the observed particle and heat losses.

The possibility that there exist smaller (but numerous) island chains which escape detection because of their size but whose effect on transport is not negligible does not seem to receive much favour. Indeed, it is difficult to justify theoretically the formation of islands of sufficiently high amplitude to cause the observed transport, and, experimentally, the nature of the observed transport seems to differ from what one would expect from the existence of such islands [2].

On the other hand, a number of theoretical studies has shown that the experimental profiles are unstable to a large class of almost-electrostatic perturbations (generally referred to as "electrostatic"), characterised by the fact that the magnetic field perturbation does not enter in the stability equations to the relevant order. The "drive" of this class of instabilities is a temperature and/or density gradient. From the microscopic point of view these instabilities involve the bulk of the plasma and are therefore mainly "fluid" in nature (as opposed to the class of weaker "kinetic" instabilities which rely on a small population of resonant particles). Broadly speaking, these instabilities are the plasma analogue of the universally occurring gradient-driven instabilities which lead to the onset of convection and to convective turbulence in many physical systems.

In the past few years most of the work on microturbulence has been focused on various versions of the ion temperature gradient (ITG) model. While this model cannot address the issue of particle transport (because it relies on the assumption of adiabatic electron response) and the electron thermal transport is only qualitatively correct, the ion heat transport can be calculated accurately in many physically relevant parameter regimes. This is the priority goal, since ion thermal transport contributes dominantly to the total energy losses in the present large devices, at least in the operation regimes of current interest.

For a general recent discussion of the present knowledge and of some open key questions in ITG turbulence theory we refer the reader to Ref. [3]. In the following, we recall only those aspects that are employed in the construction of our transport model.

We start with the reasonable assumption that the radial correlation length of turbulence λ_c is much smaller than the minor radius a. If this is the case, transport over an intermediate scale l such that $\lambda_c << l << a$ is governed by diffusion equations (a similar inequality should also be applied to the corresponding timescales). Note that this does not rule out the possibility that certain transient processes exhibit nondiffusive behaviour, if the above condition is violated.

Next, one is tempted to assume that the thermal conductivity depends parametrically only on the local features of the ambient turbulence. We therefore consider the general form

$$\chi_i = (\lambda_c^2 / \tau_c) f(v_E \tau_c \lambda_c), \qquad (1)$$

where τ_c is a characteristic time – e.g., the local correlation time, v_E is the characteristic **E** x**B** velocity fluctuation and $f(x)$ is some function.

It is usually assumed that v_E is of order λ_c / τ_c so that the function f is replaced by a constant. This seems plausible, unless strong coherent structures are present, which are characterised by high values of the rotation number $R_E = v_E \tau_c/\lambda_c >>1$. Experimental determination of R_E is difficult, due to the uncertainty in the measurement of v_E. In TEXT, values in the range $1 < R_E < 10$ were observed. Thus, in the following, we take $f(x) = 1$ but we allow τ_c to vary to be consistent with the experimental trends. This is equivalent to impose that τ_c is the actual correlation time and to simultaneously choose the residual parametric dependence embodied in $f(x)$ to match the experimental observations.

We now turn our attention to the correlation length. In order to evaluate λ_c, we invoke two more assumptions about the turbulent dynamics.

First we assume that a sizeable fraction of the turbulent energy cascades from the injection scale towards larger scales until it reaches some longwave-length cut-off. As a result one expects a peak of the turbulent energy spectrum in that region. Note that this inverse cascade process is expected on general grounds on the basis of the two dimensional convective nonlinearities present in the ITG model. The inverse cascade is well documented in the results of direct numerical simulations both with hydrodynamical models and particle simulations.

The large scale cut-off of the ITG model is set by the ion Landau damping. In toroidal geometry the condition for marginal stability reads [3].

$$\omega_{*T} \approx k_{\|}^{eff} c_s, \tag{2}$$

where $\omega_{*T} = (cT_e / eB)(k_\theta / L_T)$ is the drift frequency associated with the ion temperature gradient scale length L_T, $k_{\|}^{eff}$ is some effective parallel wavelength, $c_s = (T_e / m_i)^{1/2}$ is the ion sound speed, T_e is the electron temperature, B the toroidal magnetic field and k_θ the poloidal wavenumber.

For short wave-length modes one can estimate $k_{\|}^{eff} \approx 1 / (qR)$ where q is the local safety factor and R the major radius. The distance qR can be taken as the effective parallel length of the system since it is the distance along the field line between the outer portion of the torus, whose unfavourable curvature makes it locally unstable to the interchange branch, and the inner torus, which is locally stable. In the electrostatic drift modes of the type driven by the ion temperature gradient the propagation time of the ion acoustic wave over this distance, qR/c_s, is the fundamental time for the change of the stability properties. Instability suppression is achieved when this time is shorter than the timescale for the instability to develop.

From Eq. 2 one then obtains the estimate for the large scale poloidal cut-off of the turbulent spectrum.

$$k_{\theta cut-off} \approx L_T / (qR\rho_s). \tag{3}$$

Note that unstable modes with effective parallel wavelength smaller than 1/(qR) can exist [4]; they therefore violate condition 3. However the corresponding growth rate is very small and we assume that their contribution to the total turbulent transport is negligible. In doing so, one is supported by the experimental evidence that the roll-over of the fluctuation spectrum does indeed occur at $k_\theta \rho_s \approx 0.1$, in agreement with Eq. 3.

The second assumption is that the turbulent spectrum is isotropic, so that the radial correlation length is comparable to the poloidal one. Isotropization of the turbulent spectrum is commonly observed in numerical simulations, from the simplest two-dimensional simulations (as an example, see Ref. [5]) to the most recent full-torus particle simulations [6, 7]. A mechanism of isotropization based on secondary instabilities has been proposed and analysed by Cowley *et al* [8]. According to this work, anisotropic (say, elliptical) structures are unstable because of the strong gradients experienced in the direction of their minor axis. This causes a gradient drive analogous to the primary ITG instability drive. Qualitatively, the resulting structures must be roundish in order to be robust to secondary instabilities.

Combining isotropization with Eq. 3 one obtains an estimate for the radial correlation length:

$$\lambda_c \approx \rho_s (qR / L_T). \tag{4}$$

The characteristic time τ_c is related to the turbulent energy injection rate which in turns is linked to the growth rate of the ITG instability. Since the dominant branch is interchange-like (curvature-driven) one, we take, for $k_\theta \rho_s < 1$,

$$\gamma \approx v_i (k_\theta \rho_s) / (RL_T)^{1/2}, \tag{5}$$

where $v_i = (T_i / m_i)^{1/2}$ is the ion thermal velocity. The growth rate reaches a maximum at $k_\theta \approx 1/\rho_s$ and then rolls over.

At this stage, however, there is still some uncertainty at what value of k_θ one should evaluate γ in order to estimate τ_c. In simple single field models of plasma turbulence like the Hasegawa-Mima equation [9] the spectral density of energy injection ε_k is usually proportional to the spectral energy density $\varepsilon_k \sim \gamma(k_\theta)|\phi_k|^2$. When a strong inverse cascade is present, the wavenumber dependence of the spectral energy density (which is peaked low k's) is so strong [10] that it-more-than compensates the wavenumber dependence of $\gamma(k_\theta)$ for the usual growth rate models. The result is a shift of the peak of ε_k to the low-k cutoff region.

On the other hand, the spectral density of energy injection in a multifield turbulence model like ITG involves the cross correlation between two fields, e.g. - the potential fluctuation injection rate would depend on quantities like $\phi \partial_\theta T_i$ as one can obtain from Eq. 15 below. Thus it is difficult at this stage to determine a priori where the injection peak would occur.

If one estimates τ_c as the inverse of γ by taking k_θ from Eq. 3, as the Hasegawa-Mima example would suggest, one would obtain

$$\chi_i \sim (cT_e / eB)q(\rho i / L_T)(R / L_T)^{1/2}$$

where ρ_i is the ion Larmor radius. However this expression has the drawback that, because of the first power of q, it predicts a too weak scaling of the energy confinement time with current. Detailed scaling experiments in JET [11] as well as scaling law studies from the ITER data base [12] suggest a stronger dependence. This difficulty is removed if one estimates the characteristic time as the inverse of the maximum growth rate, $\tau_c \approx (RL_T)^{1/2} / v_i$. This choice introduces a q^2 scaling in the conductivity, as well as the property that the conductivity is radially increasing, as discussed in the following section. One then obtains

$$\chi_i = C_i(cT_e / eB)q^2(\rho_i / L_T)(R / L_T)^{3/2}, \tag{6}$$

where C_i is a constant to be determined empirically.

In order to close the model one needs to introduce a thermal conductivity for the electrons. At this stage, we adopt the strongly simplifying assumption that the electron heat is carried only by the trapped electrons. We then assume the expression

$$\chi_e = C_e(cT_e / eB)(r / R)^{1/2}q^2(\rho_i / L_T)(R / L_T)^{3/2}, \tag{7}$$

where one can see that, besides the new multiplicative constant C_e, the only difference with the expression for χ_i is the trapped electron fraction $(r/R)^{1/2}$. This is a reasonable assumption in the outer half radius, but it is obviously too rough when modelling transport near the plasma core, since then $\chi_e \rightarrow 0$.

Obviously, this will cause the model to overestimate the electron temperature in the centre, as it will be shown in Section 4.

Finally, we stress that the model presupposes that the system is not close to marginal stability where a threshold function of the regulating factor $(R/L_T - R/L_{T,crit})$, where $L_{T,crit}$, is the critical (threshold) temperature scale length, would appear in Eqs. 6-7. A thorough analysis [13] of the TFTR pellet experiment [14] has shown that the machine does not operate close to the ITG threshold in the transport zone. This conclusion is supported by other experiments, such as JET. This is not too surprising: even if a threshold function had been included (as in Ref. [15] for example), it would affect the transport analysis only near the core where temperature gradients are weak. Since the gradients become progressively steeper as one approaches the edge (and even more so as the input power is increased), the use of a threshold function can be neglected for most of the practical purposes. From a more fundamental viewpoint, the notion of threshold seems also in conflict with the idea of turbulence. The latter requires the excitation of a large number of degrees of freedom, whereas around threshold only

few modes should be active. Thus, even if a tokamak were operating near threshold (as it may perhaps happen in the recently discovered shear reversal regimes), the very use of a transport model based on the diffusive approximation (which requires a well-developed turbulent regime) would be unfeasible in this circumstance.

3. PROPERTIES OF THE MODEL

One can see that the transport model given by Eqs. 6 and 7 belongs to the general class of the so-called gyro-Bohm models. As such, the global temperature scaling of the thermal conductivity is $\chi \sim T^{3/2}$. In order to estimate the scaling law of the confinement time it is convenient to assume that the plasma is sufficiently collisional that $T_e \approx T_i$ and that ion losses are dominant as suggested by the difference in the aspect ratio dependence between χ_i and χ_e. Then, upon using Eq. 6 in the balance equation one obtains

$$\frac{P}{naR} \sim \chi_i \frac{\partial T_i}{\partial r} \sim \left(\frac{cq}{eB}\right)^2 T_i^{5/2} m_i^{1/2} (R/a)^{3/2} (1/a^2), \tag{8}$$

where P is the input power and L_T has been replaced with a as it would follow from the spatial integration. One then estimates the confinement time τ_E as

$$\tau_E \sim \frac{nT_i a^2 R}{P} \sim (P/n)^{-3/5} (eI_p/c)^{4/5} m_i^{-1/5} R^{4/5} a^{7/5}, \tag{9}$$

where the plasma current I_p has been introduced.

It is important to note that a different scaling could be appropriate in certain operational regimes where temperature equilibration does not apply. In general, the actual scaling would depend also on the collisionality regime and on the heating method. Thus, inspection of the χ_i expression shows that the ion component has per se a weaker than Bohm dependence on T_i. This might explain the result of some transport studies that attempted a separate evaluation of the losses through the ion and electron channels [16].

An important property of our model is made apparent when one considers the spatial dependence of the temperature profile. Upon assuming a power-law dependence on the distance x from the edge, $T_i \sim x^\alpha$, and using the balance equation 8 one verifies that $\alpha = 7/5$, since the left hand side (LHS) can be taken as constant. This implies that $\frac{\partial T_i}{\partial r} \sim x^{2/5}$ or that $\chi_i \sim x^{-2/5}$. Thus the thermal conductivity increases approaching the edge, in line with the experimental observations and contrary to what is often through to be a necessary property of the ITG models. This is in addition to the contribution that comes from the spatial dependence of the safety factor. Note also that the correlation length increases as 1/x. Long correlation lengths near the plasma edge are considered necessary, on phenomenological grounds, in order to

explain the behaviour of the heat conductivity. This has led to suggestions that extended radial structures that lead to a Bohm-type conductivity dominate near the edge. Here we offer an alternative possibility: that transport is still gyro-Bohm near the edge, but that the correlation length adjusts in such a way that the conductivity increases. One can easily realise that this property is shared with any model of the form $\chi_i \sim T^{\mu} L_T^{-\nu}$ provided that $\mu < \nu$ (or possibly even when $\mu = \nu$ as a consequence of the dependence of χ_i on the other parameters).

We now show that the model is consistent with dimensional analysis. Consider a simplified equilibrium with circular flux surfaces. We restrict the analysis to an annulus located between two radii, say $r = a'$ and $r = a$ ($a' < a$). We again denote by x the radial coordinate. Under the assumption that the radial turbulence correlation length is small, a' and a should not enter in the relevant dimensionless parameters. However the minor radius r at the radial location of interest is a relevant length as it is a measure of the circumference of the magnetic surface. So r effectively sets a length in the poloidal direction. We use r as the natural length unit.

The appropriate boundary condition (b.c.) for this problem is a flux b.c. at $r = a'$. That is, we impose $Q = -\chi_i \frac{\partial T_i}{\partial r}$ at the inner boundary. Dimensionally, this implies $Q = \overline{T} r / \tau$ where $\overline{T}$ and τ are the temperature and time units, respectively. A relation between these units is also obtained by imposing $(c\overline{T}/eB) = r^2/\tau$. One obtains the set of units:

$$\begin{aligned} & r && \text{length,} \\ & \tau = (cQ/eB)^{-1/2} r^{3/2} && \text{time,} \\ & \overline{T} = (eBQr/c)^{1/2} && \text{energy.} \end{aligned} \tag{10}$$

This set of units looks somewhat unfamiliar, but it is the natural one with flux b.c.'s. Note that the temperature of the two species cannot be used as units since they are dependent variables whose relation with the input power is a priori unknown. Note also that no assumption about the scaling of the radial correlation length is made, except that it is small.

With the units Eq. 10 one can construct a set of dimensionless parameters. For the ITG model a convenient set is

$$\overline{\rho}_* = (\overline{T} / m_i)^{1/2} / \omega_i r \qquad \text{effective } \rho_*, \tag{11}$$

$$\varepsilon = r/R \qquad \text{inverse aspect ratio,} \tag{12}$$

$$q \qquad \text{safety factor,} \tag{13}$$

$$\hat{s} = r d\ln q/dr \qquad \text{shear.} \tag{14}$$

Note that β is not included in the set of dimensionless parameters because of the electrostatic nature of the ITG model. The collisionality parameter in the form $\nu_{ii}\tau$ could be important near the edge, but it has been omitted for simplicity. We must also stress that the relation between the effective scale separation parameter $\bar{\rho}_*$ and the usual ρ_* depends on the actual scaling law of the temperature profile.

To show how this normalisation works in practice, we report here the (perhaps) simplest possible toroidal ITG model as obtained from a similar model of Ref. [3], by using the above units:

$$\frac{d}{dt}\left(\frac{\phi-\langle\phi\rangle}{Te}-\bar{\rho}_*^2\nabla^2\phi\right)+2\varepsilon\omega_d(\phi+T_i)+(\varepsilon/\bar{\rho}_*)\nabla_{\|}\mathbf{v}=0, \tag{15}$$

$$d\mathbf{v}/dt+(\varepsilon/\bar{\rho}_*)\nabla_{\|}(\phi+T_i)=0, \tag{16}$$

$$dT_i/dt+\Gamma\langle T_i\rangle(\varepsilon/\bar{\rho}_*)\nabla_{\|}\mathbf{v}=-(\varepsilon/\bar{\rho}_*)|T_i|^{1/2}|\nabla_{\|}|T_i, \tag{17}$$

where ϕ is the electric potential and $\mathbf{v}$ the parallel ion velocity, normalised to $\bar{T}/e$ and $(\bar{T}/m_i)^{1/2}$ respectively. The radial coordinate x is normalised to r and Γ is a constant of order one. The operators are the advection operator $d/dt=\partial_t+\mathbf{v}_E\cdot\nabla=\partial_t+\partial_x\phi\partial_\theta-\partial_\theta\phi\partial_x$, the curvature operator $\omega_d=(\cos\theta)\partial\theta+\sin\theta\partial_x$, the parallel gradient operator $\nabla_{\|}=(1/q)(q\partial\phi+\partial_\theta)$ and the flux surface averaging operator $\langle\cdot\rangle$. The operator $|\nabla_{\|}|$ in the temperature equation symbolically represents the nonlocal operator which is $|k_{\|}|$ in Fourier space, and models parallel Landau damping [17]. In writing Eqs. 15-17 we have again taken an annulus as a domain and we have neglected a weak dependence on the cylindrical metric. Thus $\nabla^2=\partial_x^2+\partial_\theta^2$. Note also that an independent equation for T_e is in principle required, although one can close the system by imposing $T_e=\langle T_i\rangle$.

The general solution for the ion temperature profile will be of the form:

$$\langle T_i\rangle=\bar{T}F(x,\bar{\rho}_*,\varepsilon,q,\hat{s}), \tag{18}$$

where F(...) is some function and we assume that the dependence on the safety factor is fully characterised by the local q and shear $\hat{s}$.

In order to make contact with the local expression for the conductivity, it is convenient to assume again a power-law dependence on the dimensionless parameters:

$$F(x,\bar{\rho}_*,\varepsilon,q,\hat{s}),\sim x^{\alpha}\bar{\rho}_*^{\beta}\varepsilon^{\gamma}q^{\delta}\hat{s}^{\varepsilon}. \tag{19}$$

Note that the temperature depends on the input power only through $\bar{T}$ and $\bar{\rho}_*$. Thus the gyro-Bohm scaling $T\sim Q^{2/5}$ corresponds to $\beta=-2/5$. Similarly one needs $\beta=0$ for Bohm

transport. Note also in general, the relation $\rho_* = \bar{\rho}_*^{1-\beta/2}$, so *if transport is gyro-Bohm*, $\rho_* = \bar{\rho}_*^{-4/5}$.

The effective local conductivity $\chi = Q/\nabla\langle T_i\rangle$ is obtained from Eqs. 18-19 by eliminating Q and by using $L_T = rx$. One can then verify that with $\beta = 2/5$ one obtains the general form of the local gyro-Bohm conductivity

$$\chi \sim \frac{cT}{eB}\frac{\rho}{L_T^a R^b r^{1-(a+b)}}, \tag{20}$$

with $a = 5\alpha/2 - 1$, $b = 5\gamma/2$ and arbitrary dependence on the other parameters.

One can verify that our model corresponds to the choice a = 5/2, b = -3/2, or, with respect to Eq. 19, $\alpha = 7/5$, $\beta = -2/5$, $\gamma = 3/5$, $\delta = -4/5$ and $\varepsilon = 0$.

4. TRANSPORT SIMULATIONS

Table 1. Machine parameters for Figures 1-11

Device	Shot n.	B_T (T)	P (MW)	I_p (MA)	n_e (10^{19} m^{-3})	Z_{eff}
JET	19649	3.	10.4	3.	2.8	2.4
JET	19691	3.	17.5	3.	3.9	3.7
TFTR	45950	4.8	11.4	2.	3.3	2.6
JT60-U	21796	2.4	5.	1.0	0.93	2.5
JT60-U	21811	4.0	11.3	1.6	1.84	2.3
D-III-D	71378b	1.	3.5	0.7	3.5	2.3
D-III-D	71384	2.	15.	1.4	8.9	2.4
ASDEX-U	31433	2.16	0.81	0.38	2.6	2.4
START	21502	0.38	-	0.096	0.25	2.

Simulations of L-mode/ohmic quasi-stationary discharges from a number of machines (see Table 1 for the plasma parameters of the selected discharges) have been carried out with the JETTO code used in a semi-interpretative way, so that particle transport is not studied and experimental density profiles are prescribed. Convective losses are not modelled and are assumed to be included in the expression for the conductive heat flux resulting from Eqs. 6-7. The coefficients C_i and C_e have been calibrated on the JET shot No. 19649. The resulting values turn out to be very close, so we take them equal:

$$C_i = C_e = 0.014 \tag{21}$$

In addition to the present model, profiles obtained with two empirical models previously tested against JET are also presented. These are a Bohm model [18, 19]:

$$\chi_e = C_B \frac{cT_e}{eB} L_{pe}^{*-1} q^2, \tag{22}$$

$$\chi_i = 3\chi_e, \tag{23}$$

$$L_{pe}^{*} = p_e / (a|\nabla p_e|), \tag{24}$$

$$C_B = 2. \times 10^{-4}, \tag{25}$$

where p_e is the electron pressure, and the following gyro-Bohm model [20]

$$\chi_e = C_{gB} \frac{cT_e}{eB} L_{pe}^{*-1} \rho_* q^2, \tag{26}$$

$$\chi_i = 2\chi_e, \tag{27}$$

$$C_{gB} = 0.18. \tag{28}$$

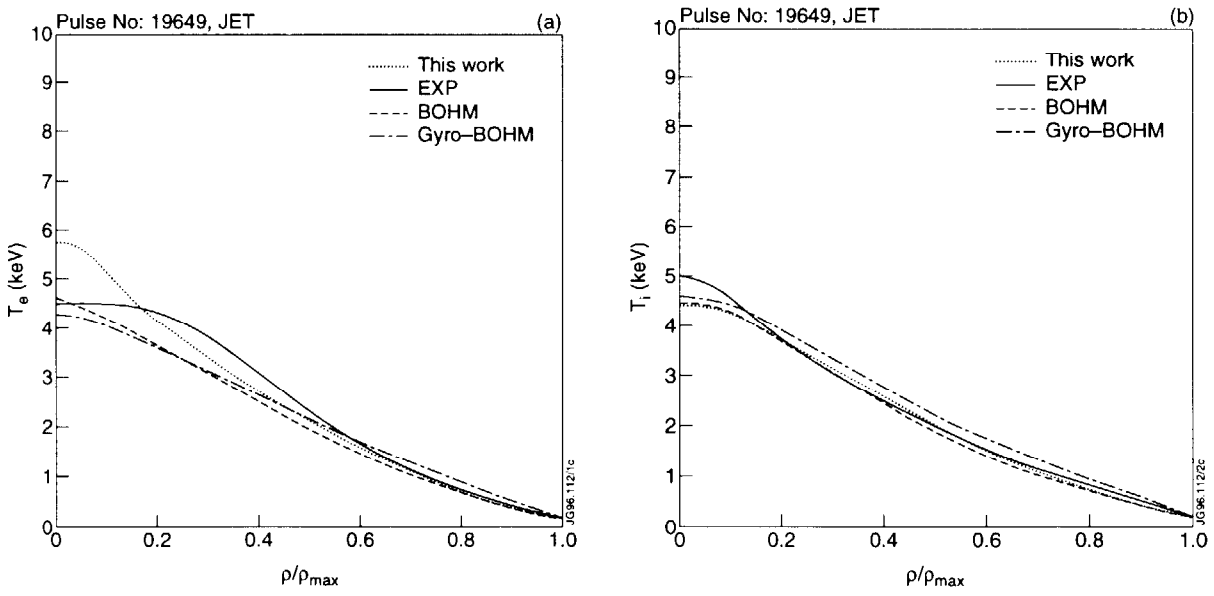

Fig.1: Calibration Case. JET shot n. 19649. (a) Electron and (b) ion temperature. Solid line, experiment; dotted line, this work; dashed line, Bohm model; dash-dotted line, gyro-Bohm model.

The result for this calibration shot is shown in Figure 1. Note that here and in subsequent figures (a) refers to the electron temperature and (b) to the ion temperature; we employ solid lines for the experimental profiles, dotted lines for the model given by Eqs. 6-7, dash lines for the Bohm model (Eqs. 22-23) and dash-dotted lines for the gyro-Bohm model (Eqs. 26-27).

After calibration the model was tested successfully against another JET discharge (n. 19691, see Figure 2) which represents a power scan experiment with respect to the calibration shot.

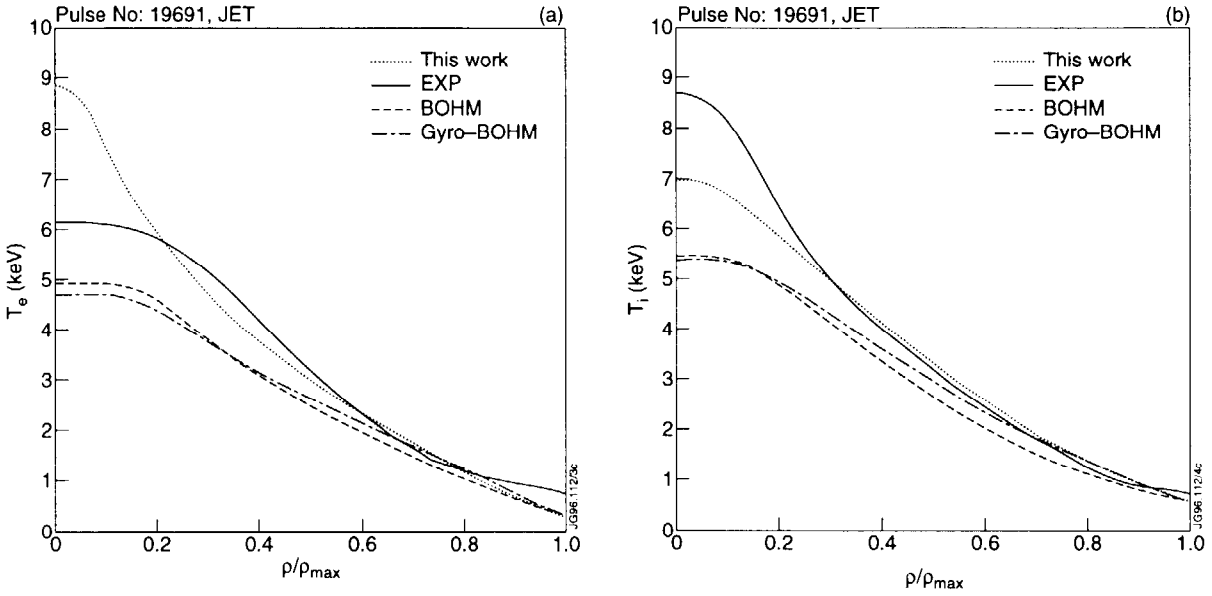

Fig.2: JET Shot n. 19691. (a) Electron and (b) ion temperature. Line codes as in Fig. 1.

The subsequent figures show the results of the simulations of discharges of various machines whose plasma parameters can be very different from JET. In this respect, we stress that the coefficients of the models are not recalibrated when simulating the other machines. Our simulations include a typical L-mode discharge in TFTR [21] (Figure 3), $\rho*$-scaling

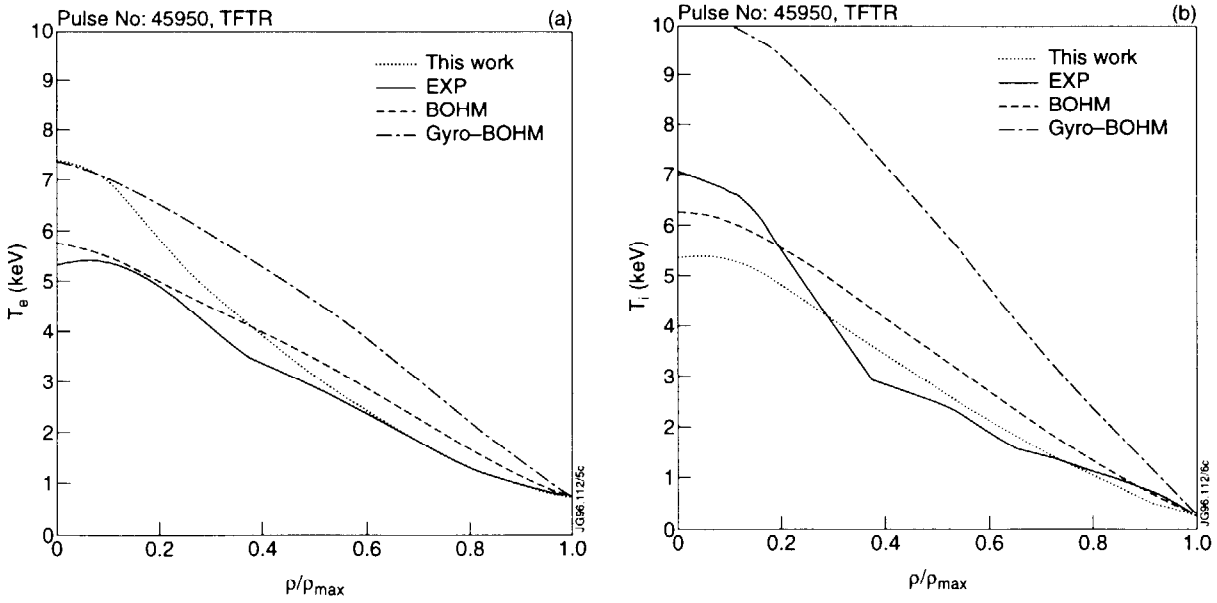

Fig.3: TFTR shot n. 45950. (a) Electron and (b) ion temperature. Line codes as in Fig. 1.

experiments in JT60-U [21] (Figures 4-5) and D-III-D [21] (Figures 6-7), an L-mode discharge in ASDEX-U [20] (Figures 8a) and an ohmic START discharge [22] (Figure 8b). Figure 8 refers to the electron temperature only.

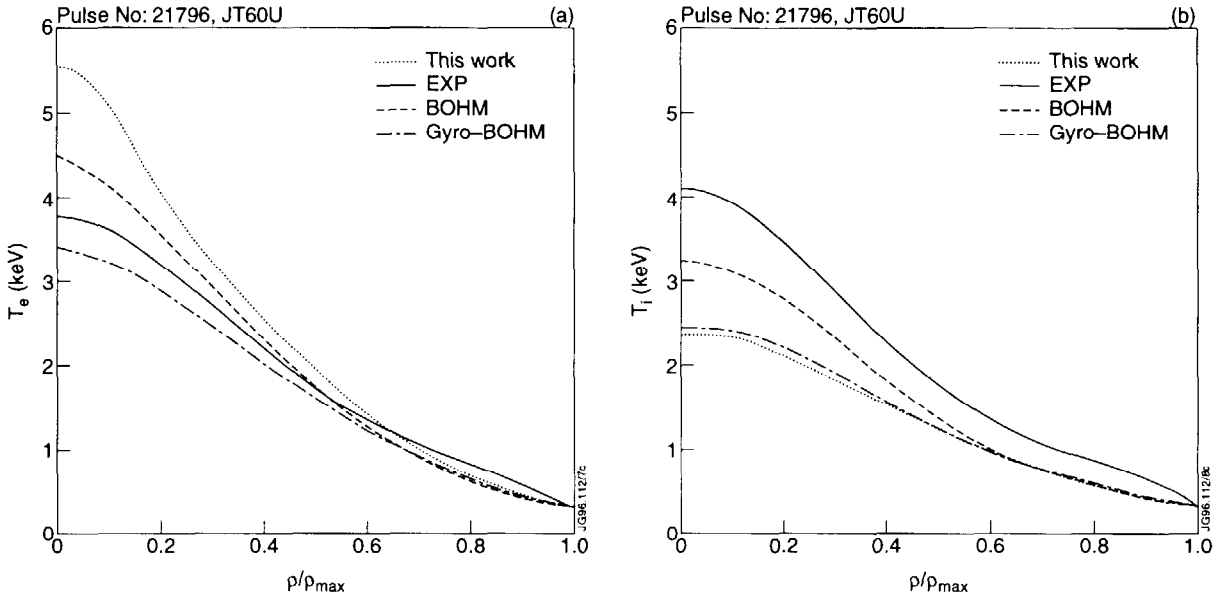

Fig.4: JT-60-U shot n. 21796. (a) Electron and (b) ion temperature. Line codes as in Fig. 1.

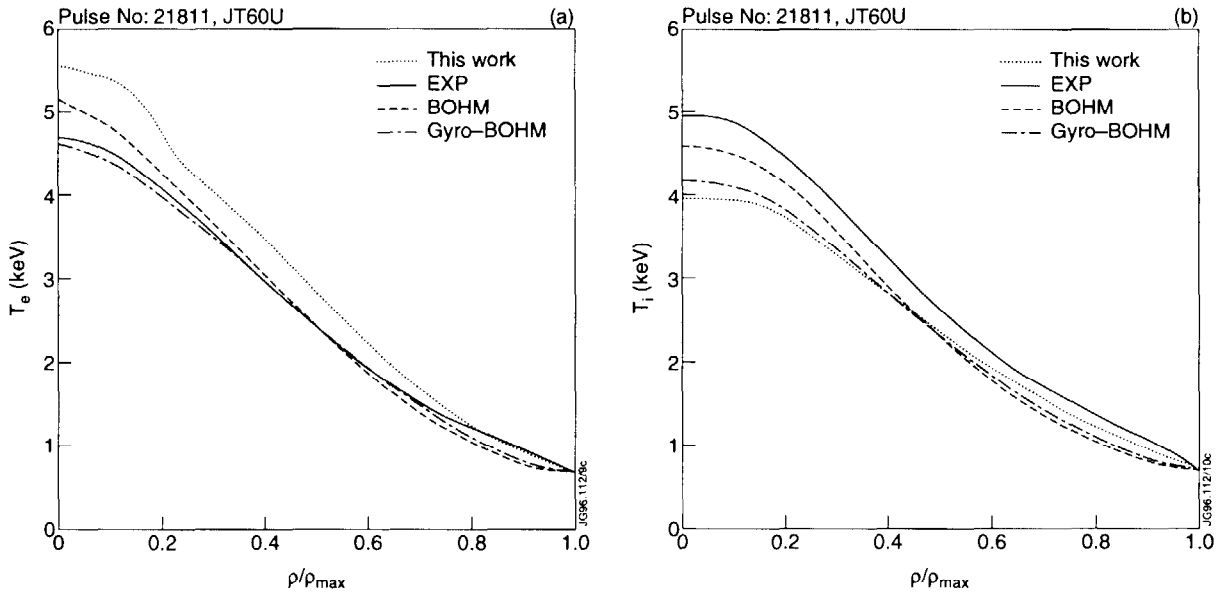

Fig.5: JT-60-U shot n. 21811. (a) Electron and (b) ion temperature. Line codes as in Fig. 1.

The overall performance of the model when applied to the large machines is reasonably good in the outer half radius and, on the average, better than the standard Bohm or gyro-Bohm models. In the core the model systematically underestimates the electron transport and overestimates the ion transport. In smaller machines the best agreement is achieved by the gyro-Bohm model, a known fact [23, 24].

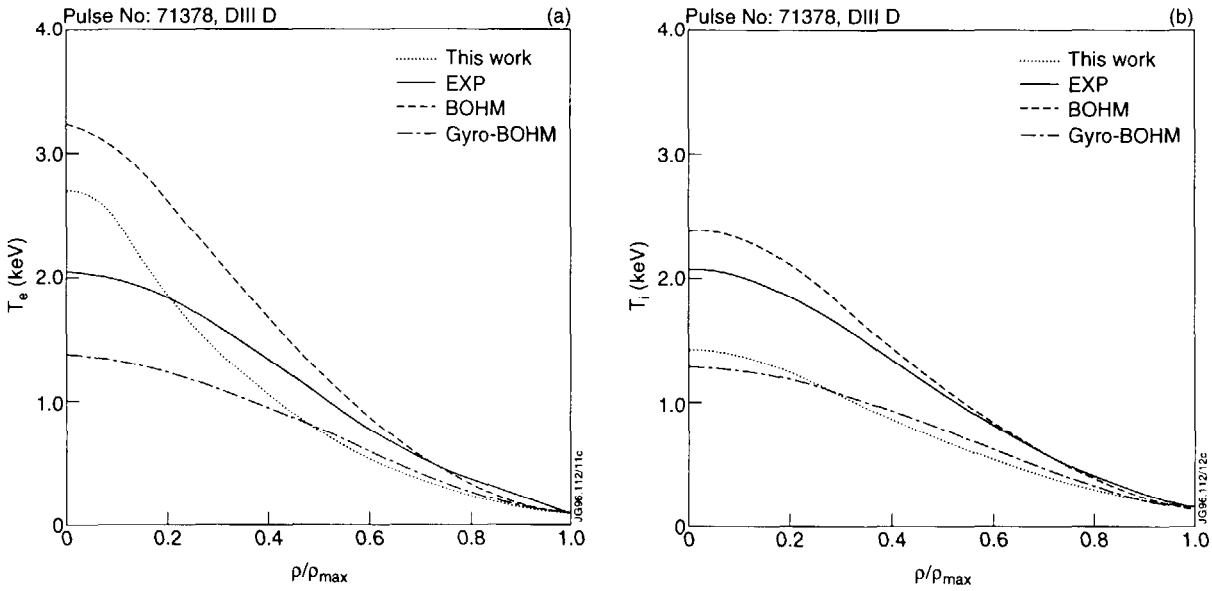

Fig.6: D-III-D shot n. 71378b. (a) Electron and (b) ion temperature. Line codes as in Fig. 1.

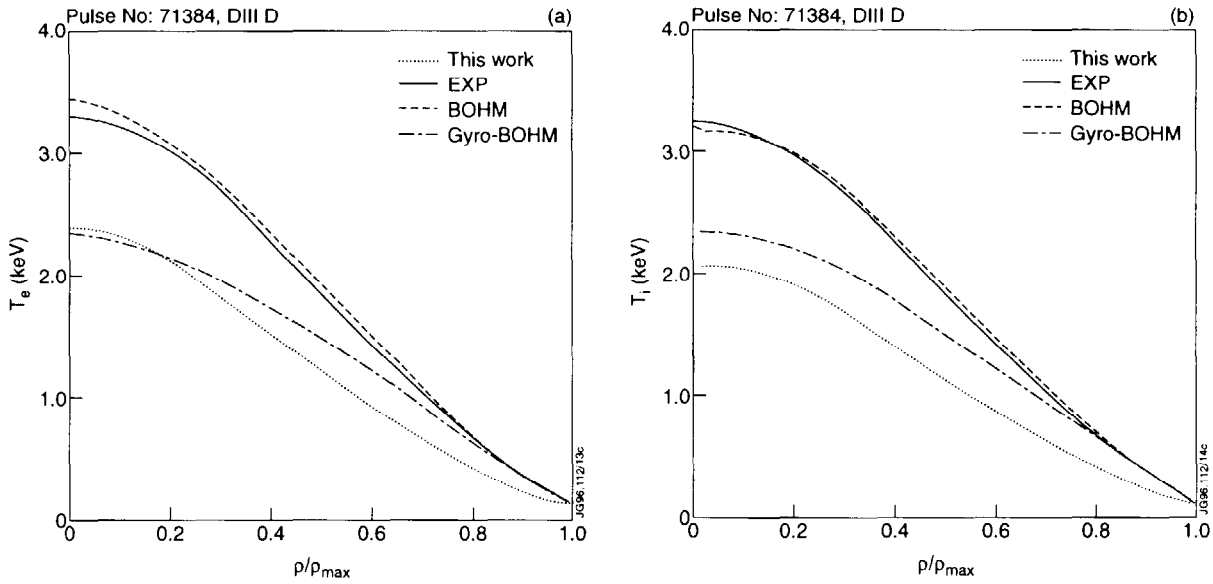

Fig.7: D-III-D shot n. 71384. (a) Electron and (b) ion temperature. Line codes as in Fig. 1.

The electron behaviour in the core can be understood if one allows for the crudeness of the modelling (some contribution to transport from the passing particles is expected even when the fraction of trapped particles goes to zero). In some cases the presence of sawteeth is also a factor. Indirectly, underestimating the electron conductivity causes the ion conductivity to be overestimated, since χ_i increases with T_e, thus accounting for the systematic behaviour of T_i in the core.

In the case of ions one should also stress again that the model is meant to work well above the ITG threshold, where ITG is particularly virulent and where a minimal number of control parameters is expected to play a role. (Hence the applicability of the model to L-mode

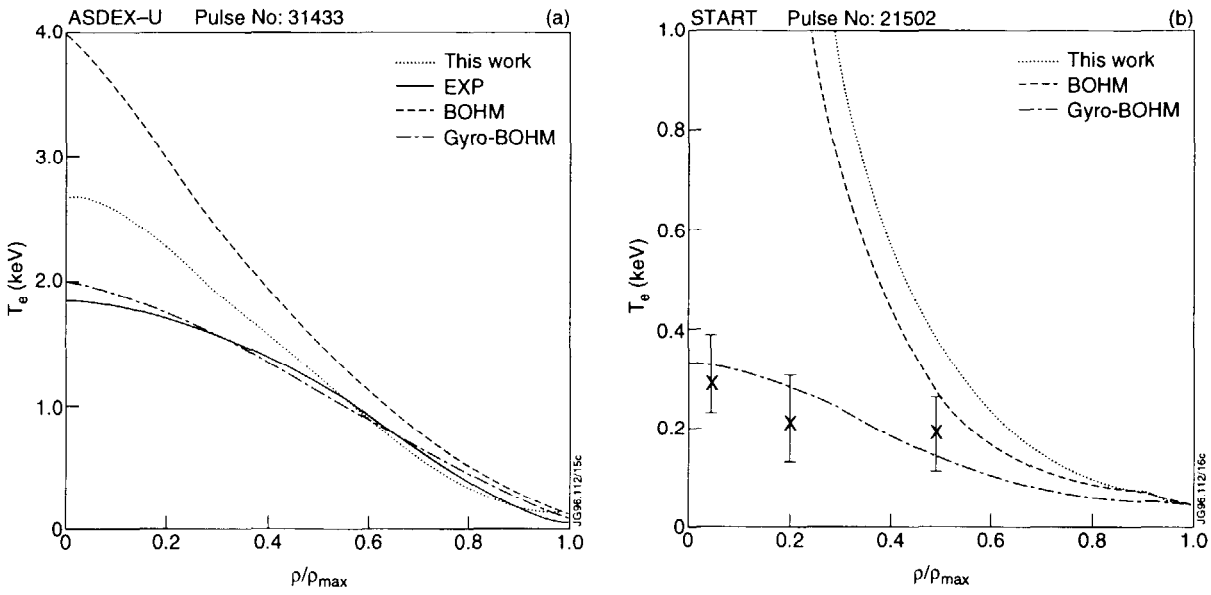

Fig.8: (a) ASDEX-U shot n. 31433 (electron temperature) and (b) START n. 21502 (electron temperature). Line codes as in Fig. 1.

discharges.) This requires L_T to be somewhat smaller if not much smaller than R. Near the core the ITG turbulence is effectively stabilised, at least in its most robust form. In addition, the stabilising role of the density gradient in certian types of discharges should also be taken into account. As employed by many authers [15, 25, 26], all of this near-marginality effects can in principle be taken into account (phenomenologically, see remarks at the end of Sec. 2) by modifying the growth rate, Eq. 5, to include a threshold function G(M) of the regulating factor $M \equiv R/L_T - R/L_{t,crit}$, where $G(M) \sim M$ for $M << 1$ (as it follows from bifurcation analysis near threshold) and $G(M) \sim M^{1/2}$ for $M >> 1$ (to match Eq. 5 in this limit).

Additional control parameters can be important in other regimes of operation. One of these is a measure of shear flow, which can be embodied in the dimensionless parmeter $L_S V_E'/c_S$, where $L_S = (qR)/\hat{s}$ is the magnetic shear length, important for weak and reversed shear discharges and the finite beta stabilisation in the core of the high beta-poloidal discharges. The effect of rotation can be seen from the D-III-D shots (Figs. 6-7) where it is apparent that our model gives consistently more transport than observed. We tentative attribute the good performance of D-III-D to the stabilising role of high shear-flow coming from unbalanced beam injection. The role of shear-flow will be considered in further developments of this basic model.

We have also carried out a direct comparison of the experimental conductivities obtained from power balance analysis with the conductivities evaluated from the model, Eqs. 6-7 with calibration constants of Eq. 21, by employing the experimental temperature profiles. Results are shown in Figures 9-11 for the JET and TFTR shots. Here a solid line represents the power-balance conductivity, a dotted line identifies the conductivity obtained from the model (marked EXP) and a dashed line shows the predictive JETTO results, as a comparison.

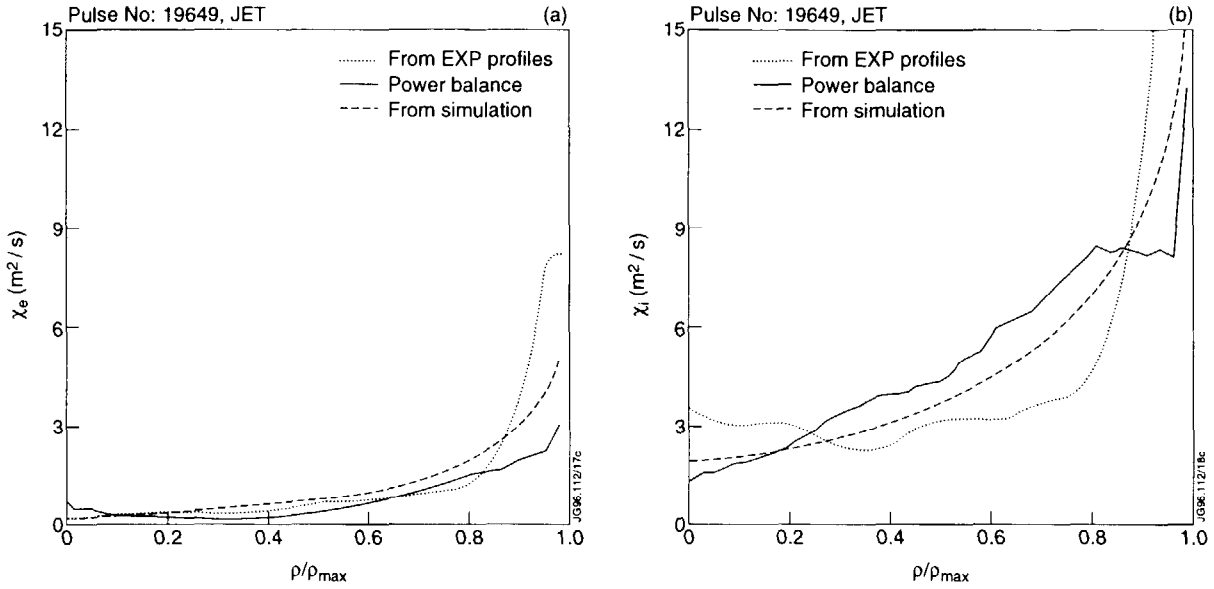

Fig.9: (a) Electron and (b) ion thermal conductivity, JET shot n. 19649. Solid line, power balance analysis; dotted line, this work, using the experimental profiles; dashed line, JETTO simulations.

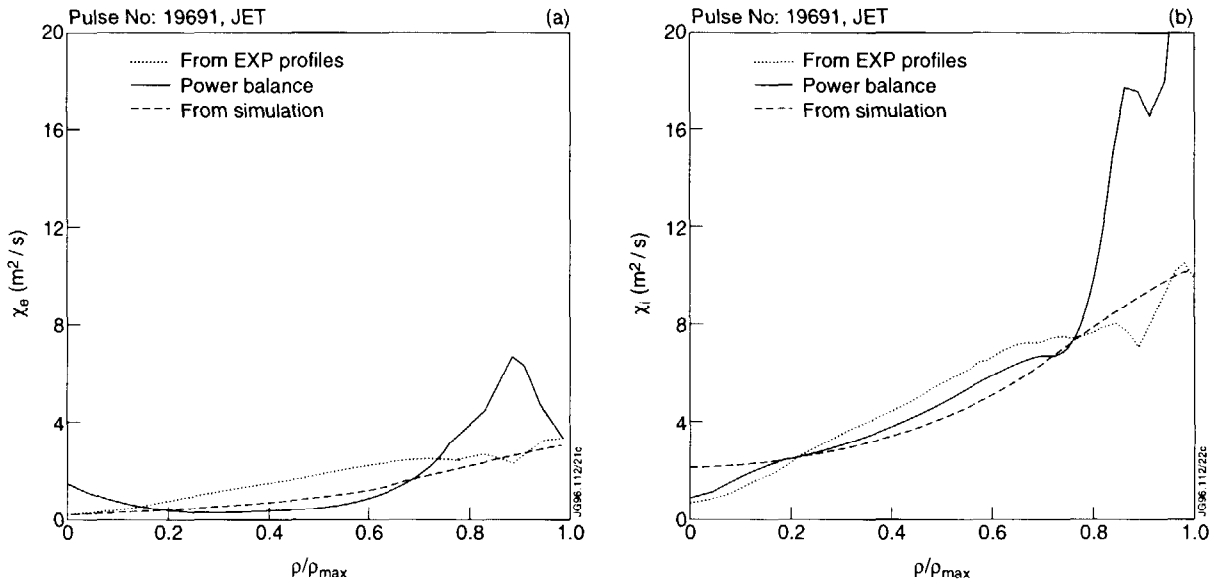

Fig.10: (a) Electron and (b) ion thermal conductivity, JET shot n. 19691. Line codes as in Fig. 9.

This is a particularly difficult test as results are affected by the experimental errors. A feature of this kind of analysis is that the deviations of the power balance conductivity tend to be anticorrelated with the deviations of the conductivity obtained from the model. This is due to the fact that, for example, a positive error on the temperature gradient will cause a reduction in the power balance conductivity (which is inversely proportional to the gradient) and a simultaneous increase in the conductivity evaluated from the model.

Nevertheless the outcome of the analysis is satisfactory. It is remarkable that the model conductivity maintains the property of being an increasing function of the minus radius. We

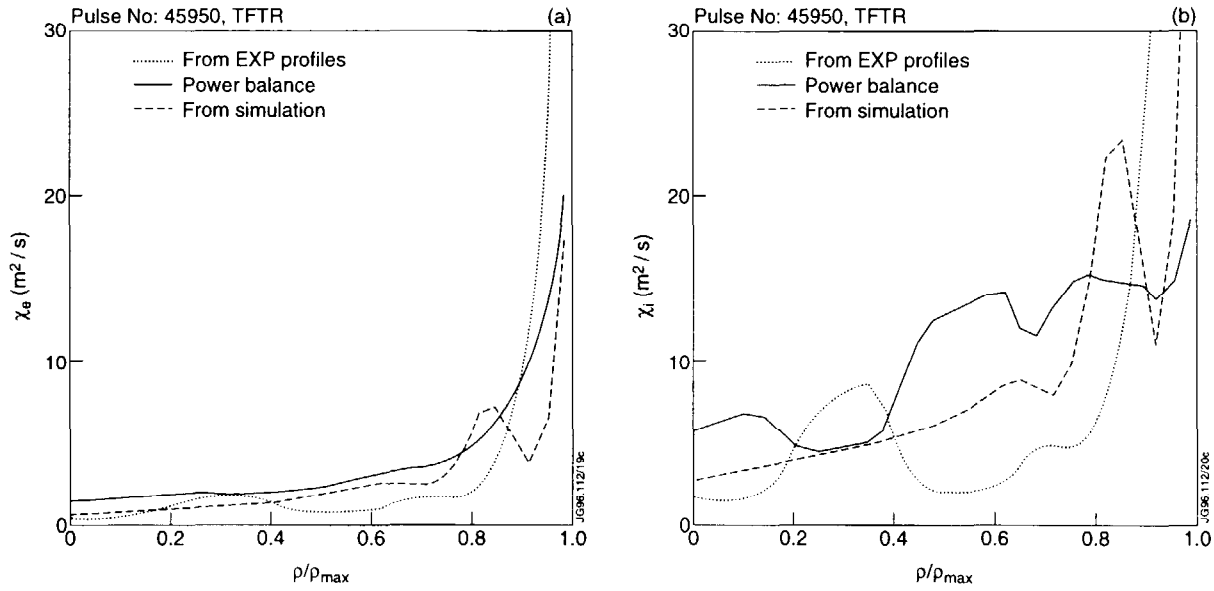

Fig.11: (a) Electron and (b) ion thermal conductivity, TFTR shot n. 45950. Line codes as in Fig. 9.

stress that this is a truly independent test of the radial dependence of the conductivities, since the temperature and the gradients are treated as independent quantities. This differs from the predictive analysis where they are functionally related (being solutions of a differential equation, the temperature and its gradient must adjust to the heat flux) and the radial dependence is, in a sense, "built in", as discussed in Section 3.

5. CONCLUSIONS

To summarise, we have presented a new model of thermal transport due to ITG turbulence which is obtained by combining the semi-quantitive knowledge drawn from the general theory and from the numerical simulations with some experimental observations.

The new model has the remarkable property that the turbulence correlation length and the thermal conductivity are growing functions of the minor radius even in the edge region. In this, our model differs from other models which rely on the threshold function to explain the growth of the conductivity with minor radius. For example the model of Refs. [26] shows initially an increase of χ_i as one goes above marginality, but then it decreases when one further approaches the edge since the temperature dependence becomes the dominant factor (μ = 3/2 while ν = 1/2, see the discussion in Sec. 3). As a consequence the model of Ref. [26] starts behaving badly typically around r/a $\approx$ 0.8, where one is then forced to impose the boundary conditions. By examining the derivation of this as well as previous, simpler models built along the same lines [25] one can see that Refs. [25, 26] are equivalent to the use of quasilinear theory in the estimate of the condicutivity, which means implicitly assuming that the correlation length is approximately ρ_s, thus independent of the temperature scale-length. Conversely, our model

exploits the inverse cascade argument, a nonlinear effect, to bring in the positive dependence of the correlation length on the temperature gradient exhibited in Eq. 4.

When compared with the experimental profiles of L-mode discharges of large machines the model performance is reasonably good (and indeed better than previous phenomenological models) in the outer half radius where ITG turbulence is expected to be more robust.

Perhaps the most important conclusion of this work is that a gyro-Bohm model like Eqs. 6-7 with a strong dependence on the temperature scale length can predict profiles that are very similar to Bohm models. This result throws a new light on the Bohm/gyro-Bohm conundrum, showing that the dependence of the transport coefficients on parameters other than $\rho*$ can play a very important role in determining the performance of a transport model.

ACKNOWLEDGEMENTS

The authors enjoyed many instructive interactions with the participants in the 1995 ITP Workshop on Turbulence and Intermittency in Plasmas, where the work was started. In particular, stimulating discussions with M. Beer, S. Cowley, J. Krommes and A. Taroni are gratefully acknowledged.

This work was supported in part by the National Science Foundation Grant No. PHY94-07194 and in part by U.S. Dept of Energy Contract DE-FG05-80ET-53088.

REFERENCES

[1] A. Cenacchi and A. Taroni, JETTO: *A free boundary plasma transport code (basic version)*, ENEA Report RT-TIB-88(5) (1988).

[2] A. Wootton et al., Proc. of the 15th International Conference on Plasma Physics and Contr. Nuclear Fusion Research, paper IAEA-CN-60/A2-4-P-9, IAEA (1994).

[3] M. Ottaviani, M.A. Beer, S. Cowley, W. Horton and J. Krommes, *Unanswered Questions in Ion-Temperature-Gradient-Driven Turbulence,* in Proceedings of the ITP program on "Intermittent and Turbulent Phenomena in Plasmas". JET Report JET-P(95)70

[4] L. Chen, S. Briguglio and F. Romanelli, Phys. Fluids **B3**, 611 (1991).

[5] M. Ottaviani, F. Romanelli, R. Benzi, M. Briscolini and S. Succi, Phys. Fluids **B2**, 67 (1990).

[6] H.E. Mynick and S.E. Parker, Phys. Plasmas **2**, 2231 (1995).

[7] Y. Kishimoto, T. Tashima, W. Horton, M.J. Le Brun and J.Y. Kim, IFS report n. 711 (1995), Phys. of Plasmas **3**, 1289 (1996).

[8] S.C. Cowley, R.M. Kulsrud and R. Sudan, Phys. Fluids **B3**, 1803 (1991).

[9] A. Hasegawa and K. Mima, Phys. Rev. Lett. **39**, 205 (1977).

[10] M. Ottaviani and J.A. Krommes, Phys. Rev. Lett. **69**, 2923 (1992).

[11] C.D. Challis et al., Nuclear Fusion **32**, 2217 (1992).

[12] P.N. Yushmanov et al., Nuclear Fusion **30**, 1999 (1990).

[13] W. Horton et al., Physics of Fluids **B4**, 953 (1992).

[14] M.C. Zarnstorff et al., Proc. of the 12th International Conference on Plasma Physics and Contr. Nucl. Fusion Research, 1990, Washington (IAEA, Vienna, 1991), vol. 1, p. 109.

[15] W. Dorland et al., Proc. of the 15th International Conference on Plasma Physics and Contr. Nuclear Fusion Research, paper IAEA-CN-60/D-P-I-6, IAEA (1994).

[16]. C.C. Petty et al., Phys. of Plasmas **2**, 2342 (1995).

[17] G.W. Hammett and F.W. Perkins, Phys. Rev. Lett. **64**, 3019 (1990).

[18] A. Taroni, M. Erba, F. Tibone and E. Springmann, Plasma Phys. and Contr. Fusion **36**, 1629 (1994).

[19] M. Erba, B. Parail, E. Springmann and A. Taroni, Plasma Phys. and Contr. Fusion **37**, 1249 (1995).

[20] M. Erba, E. Springmann, A. Taroni and F. Tibone, Proceedings of the Varenna Workshop on Local Transport Studies in Fusion Plasmas, Editrice Compositori, Bologna (1993).

[21] S.M. Kaye et al., Status of Global Energy Confinement Studies, Rep. PPPL-2670, Princeton Plasma Physics Laboratory, Princeton, NJ (1990).

[22] J.W. Connor *et al., Transport modelling in tight aspect ratio: testing against START ohmic data and predictions for MAST*, 22nd EPS Conf. on Contr. Fusion and Plasma Phys., Bournemouth, (1995), vol. 19C, part II, p. 205.

[23] F.W. Perkins et al., Phys Fluids **B5**, 477 (1993).

[24] J.P. Christiansen et al., Nucl. Fusion **33**, 863 (1993).

[25] F. Romanelli, Phys. Fluids **B1**, 1018 (1989).

[26] M. Kotschenreuther, W. Dorland, M.A. Beer and G.W. Hammett, Physics of Plasmas **2**, 2381 (1995).